International Conference on Space Optics—ICSO 2018

Chania, Greece

9–12 October 2018

Slit homogenizers for Earth observation spectrometers: overview on performance, present and future designs

J. Caron

B. Kruizinga

R. Vink

Slit homogenizers for Earth observation spectrometers: overview on performance, present and future designs

Jérôme Caron*[a], Bob Kruizinga[a], Rob Vink[a]

[a]TNO, Optics Department, Stieltjesweg 1, 2628 CK Delft, the Netherlands

ABSTRACT

Tropomi, successfully launched in October 2017, and Sentinel-5, with launch due in 2021, are two pushbroom spectrometers measuring Earth's radiance from a Low Earth Orbit (LEO) at a high spectral resolution. Both instruments have strongly overlapping spectral channels (UV-VIS, NIR, SWIR-3). While the Tropomi spectrometers are designed with standard slits, all Sentinel-5 channels make use of complex slit assemblies called "slit homogenizers" that aim at mitigating the slit heterogeneous illumination that results from the along track spatial non-uniformity of the observed scenes, and is known to distort the instrument spectral response function (ISRF). The similarity between the two missions will allow, in a few years from now, to evaluate the performance gain resulting from these devices. If their expected success is confirmed, slit homogenizers may become standard components of future space missions.

This paper aims at providing a comprehensive, yet as simple and accessible as possible, overview of the slit homogenizer performance. The Sentinel-5 slit homogenizers, based on two parallel mirrors will be discussed, and a new and promising family of slit homogenizer designs will be presented for the first time. The new designs offer several advantages in terms of performance and manufacturability.

Keywords: Slit homogenizer, spectrometer, Earth observation.

1. INTRODUCTION

The Instrument Spectral Response Function (ISRF) of an imaging spectrometer is traditionally computed with a convolution between three functions:

$$ISRF\left(\lambda - \lambda_0\right) = \left[Slit\left(\frac{x}{m}\right) \otimes PSF_{spectro}\left(x\right) \otimes PSF_{detector}\left(x\right) \right] \otimes \delta\left(x - \frac{\lambda - \lambda_0}{k}\right), \tag{1}$$

- Slit(x/m) is a boxcar that describes the spectrometer entrance slit opening, x is the spectral coordinate on the final image plane where the detector is located, and m the spectrometer magnification from slit to detector,

- $PSF_{spectro}(x)$ is the 1D optical PSF of the spectrometer in across-slit direction, obtained after averaging the corresponding 2D PSF over the along-slit direction,

- $PSF_{detector}(x)$ respresents the 1D response of one detector pixel (a boxcar) with possibly crosstalk effects, also averaged over the along-slit direction,

- the last convolution with a Dirac function just represents a change of variable with x being replaced by $(\lambda - \lambda_0)/k$, with λ_0 being the monochromatic wavelength of illumination, and k the linear dispersion in spectral units per length unit on detector plane (typically nm per mm).

This well-known definition of the ISRF describes the instrument response to a spatially uniform and monochromatic stimulus in the spectrometer slit. This ideal situation is easily realized in a lab for characterizing the instrument properties ; however, it unfortunately does not correspond to reality. In practice, the instrument most often observes a complex scene with both spatial and spectral fluctuations L(x,y,λ). Even after blurring the spatial variations with the satellite motion smear and telescope optical PSF, the resulting illumination at the spectrometer entrance slit usually significantly deviates from the homogeneous situation.

*jerome.caron@tno.nl; phone +31 88 866 69 85.

The real ISRF is still given with the above formula (1), but the boxcar function that represents the slit must be replaced with the real slit illumination profile. As a result, an ISRF distortion is generated, that varies both spectrally, spatially (along the slit) and in time. The distortion can be quantified, for instance by the maximum difference between a particular distorted ISRF and the nominal (homogeneous case) ISRF, relative to the peak of nominal ISRF:

$$\delta ISRF = \frac{\max\left[ISRF_{non-uniform}\left(\lambda - \lambda_0\right) - ISRF\left(\lambda - \lambda_0\right)\right]}{\max\left[ISRF\left(\lambda - \lambda_0\right)\right]}.$$ (2)

In this equation, it is assumed that the ISRFs are normalized such that their spectral integral is equal to 1. In that case, the peaks of the ISRFs are not equal to 1.

We must emphasize that this ISRF distortion is inherently very different and much harder to correct than ISRF distortions resulting from a drift of instrumental properties due for instance to thermo-mechanical effects. Such effects will show a smooth spectral and temporal variation ; by contrast, the ISRF distortions induced by scene non-uniformities vary rapidly in time, creating a quasi-random radiometric error (that has been coined "pseudo-noise"). The ISRF distortion may also vary very fast spectrally in presence of strong absorption lines: outside the absorption lines the atmosphere is transparent and scene non-uniformities due to rapid albedo changes on the ground are well visible (giving a strong ISRF distortion) while in the absorption line the atmosphere is opaque and the scene non-uniformities disappear.

This ISRF distortion was first observed with the Ozone Monitoring Instrument (OMI). In the OMI spectral bands (270-500nm) the effect is equivalent to a fast varying spectral shift, and could be corrected with simple algorithms making use of the temporally oversampled data which carry information about scene non-uniformities [1]. After OMI, similar software corrections based on temporal oversampling have been studied [2], and improved to include the account of ISRF distortion so that they can be used in spectral bands with stronger absorption. Unfortunately, it was shown that this type of "software" correction cannot be used in the SWIR where absorption bands are too strong and created by too many chemical species, including the highly variable H_2O [3]. Based on these results, for the Sentinel-5 mission a "hardware" mitigation of the effect was investigated, which lead to the invention of the slit homogenizer.

2. MIRROR-BASED SLIT HOMOGENIZER

2.1 Working principle

The mirror-based slit homogenizer (SH) was proposed during the phase A-B1 of the Sentinel-5 project. It uses two parallel mirrors placed on each side of the slit [4-5]. The original idea comes from a patent for a laser illuminator homogenizer that was developed for a micro-lithographic application [6], and was re-used for space: it is a good example of cross-fertilization between different fields. The two parallel mirrors are separated by a distance w equal to the slit width (see figure 1). They will create multiple reflections over a length L. The mirrors must have special coatings designed for high reflectance at grazing angles of incidence. If the F-number of the incoming beam is equal to F#, the range of angles of incidence that will hit the mirror spans the interval [arctan(2F#) ; 90deg].
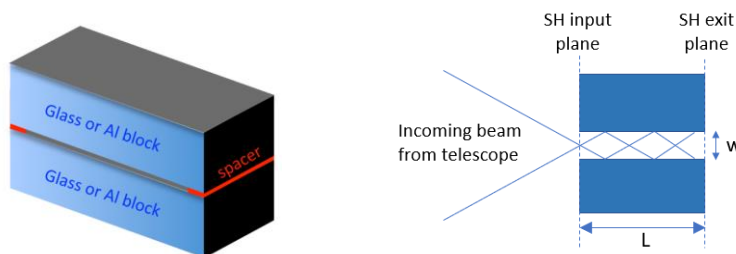

Figure 1. Left: the mirror-based SH typically consists of two blocks coated with a highly reflective coating, separated by spacers. Right: the beam delivered by the telescope is focused at the SH entrance and undergoes multiple reflections on the SH mirrors.

The slit homogenizer aims at homogenizing the illumination in the across-slit direction but must not modify the illumination in the along-slit direction to preserve the full image information along the swath. To do so, it requires an astigmatic optical system (see figure 2). In the across-slit direction, the telescope image plane coincides with the slit homogenizer input, and the slit homogenizer output, where the illumination has been homogenized, coincides with the object plane of the collimator. So the telescope image plane and the collimator object plane are separated by the distance L that is required for the homogenization to take place. In the along-slit direction, the telescope and collimator must share a common image plane and the slit homogenizer has no effect. This common image plane can be located anywhere ; if it coincides with the homogenizer input then the collimator must be astigmatic ; if it coincides with the homogenizer output the telescope must be astigmatic; in all other cases, both the collimator and telescope are astigmatic.
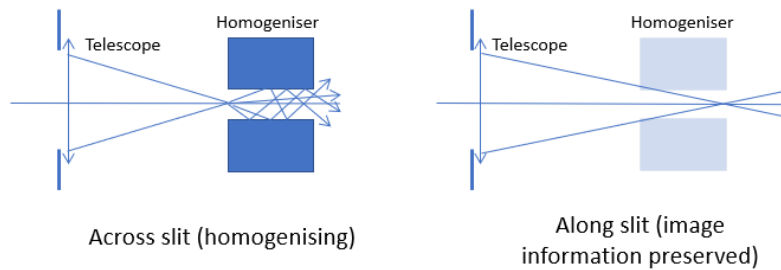

Figure 2. Left: in the across-slit direction, the telescope is focused at the SH input. Right: in the along-slit direction, the telescope focal plane can be placed at any position, the only requirement being that it coincides with the collimator object plane. In the figure, it is focused at the SH exit, which means that the telescope must have some astigmatism.

In this paper, we will describe the behavior of the mirror-based SH assuming a telecentric incident beam with chiefs rays arriving orthogonally to the slit plane. This simplified situation is of high practical relevance for pushbroom spectrometers, and corresponds to the case of Sentinel-5. The SH may be used in more general situations (non-telecentric beams) but describing its behavior becomes then increasingly complex. Note that non-telecentricity in the across-slit direction will have a limited impact: since the slit is so narrow, the variation of chief ray direction across the slit width remains usually negligible. We will also restrict our analysis to a rectangular pupil as is the case for Sentinel-5. The slit homogenizer behavior for other pupil shapes is very similar to the rectangular pupil and the SH performance can be modelled with limited adaptations.
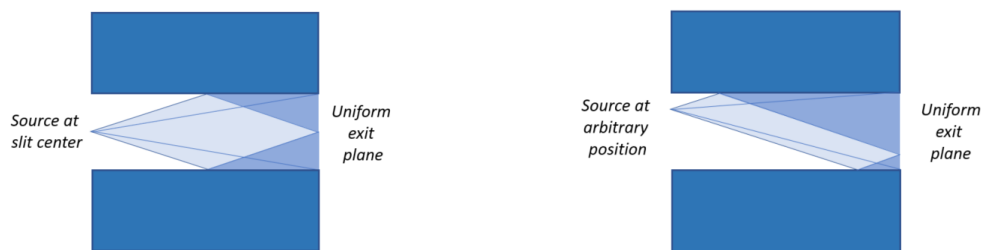

Figure 3. Illustration of the slit homogenizer length rule (equation (3)). A SH with length $L = 2wF_\#$ is represented. The beam delivered by a point source at the SH input (F-number $F_\#$ in across-slit direction, and rectangular pupil) is folded in such a way that the illumination at SH exit is uniform, for any position of the source. This interpretation based on geometrical optics is only a rough approximation.

A first-order understanding of the slit homogenizer working principle can be already obtained with geometrical optics considerations. As illustrated in figure 3 the SH mirrors will fold a beam that comes from a rectangular pupil, in a way that the intensity distribution at the SH exit will always be perfectly uniform, <u>for any position of the source point at the SH input</u>, if the SH length L is equal to an even number of times the slit width times the F-number:

$$L = 2nwF_{\#} \qquad \text{with } n = 1, 2, 3... \tag{3}$$

In reality this description of the SH is not fully correct: as we will see the multiple reflections create a complex interference pattern with strong intensity fluctuations. However, if these fluctuations are averaged out locally the obtained average intensity will follow the geometrical optics picture so that the "length rule" given by equation (3) already allows to predict a set of favorable design parameters for SH.

2.2 Performance model

We will now compute the interference pattern at the SH output and provide an accurate prediction of the SH performance. The SH is characterized by its width w, its length L and reflection coefficient R. R is defined for complex amplitudes so $|R|^2$ is the reflectance. For reflection on a perfect metal R= -1 (dephasing of π). The incoming beam has a wavelength λ_0 and a F-number F#. A transverse coordinate x is defined in the SH input plane in across-slit direction, such that x=0 at the slit center. A similar coordinate x' is defined in the SH exit plane.

We now consider an elementary source point at the SH input at the position $x=x_0$, that emits a coherent cone of light within an angle approximately equal to 1/F#. Strictly speaking, this elementary source is the image of a geometrical point on the scene observed with the telescope, and has a finite size defined by diffraction and aberrations in the telescope. Two neighboring elementary sources, even if they are very close and their light distribution overlap, are not mutually coherent since they correspond to different source points on the scene.

Two models will be presented:

1) **An interference model**, where light propagates according to laws of geometrical optics, and an interference pattern is computed based on the optical path differences between the intersecting rays. For this model, we will neglect the size of the telescope PSF and assume that the elementary source at SH input is a perfect point that emits light homogeneously within the angles defined by the F-number, and no intensity outside.

2) **A diffraction model**, where the exact light distribution of an elementary source at the SH input is considered. A good assumption is to use the equation of an Airy pattern that corresponds to a diffraction limited telescope PSF. The complex amplitude distribution at this input signal is then propagated through the SH with a diffraction integral.

Let's consider now a given position of the elementary source $x=x_0$. Due to the two parallel mirrors, this source will have an infinite number of images, that will also emit light inside an angle approximately equal to 1/F# (see figure 4). The mirror images are at the positions $x=w-x_0$, $2w+x_0$, $3w-x_0$, $4w+x$ on one side of the SH and $-w-x_0$, $-2w+x_0$, $-3w-x_0$, $-4w+x_0$ on the other side. These positions are noted x_n with $|n|$ being the number of reflections and the sign of n depending on the mirror where the last reflection takes place:
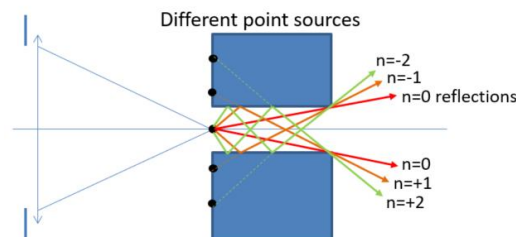
$$x_n = nw + (-1)^n x_0. \tag{4}$$

Figure 4. Multiple reflections in the SH create many images of the source point at SH input.

The observed intensity at the SH exit is a function of the exit coordinate x'. It is zero outside the slit opening (|x'|>w/2). In the slit opening (|x'|≤w/2) it is given by the following expressions:

1) Interference model

$$I_{interferences}\left(x', x_0\right) = \left|\sum_{n=-\infty}^{+\infty} f\left(x_n\right) R^n \exp\left(i\frac{2\pi}{\lambda_0}\sqrt{\left(x'-x_n\right)^2 + L^2}\right)\right|^2$$

(5)

$$f\left(x_n\right) = \begin{cases} 1 \text{ if } \dfrac{|x'-x_n|}{L} \leq \dfrac{1}{2F_{\#}} \\ 0 \text{ otherwise} \end{cases}$$

The function $f(x_n)$ determines if the mirror image of the source located at x_n can send rays that propagates inside the cone of light with angle 1/F# and will be able to reach the position x' on the image plane. The sum is infinite but in practice this function will be equal to 1 only for a few images x_n, and therefore it will limit the sum to only a few terms.

The interference model can be easily adapted to any pupil shape, by adapting the expression of $f(x_n)$ so that it takes into account the boundaries of the cone of light.

2) Diffraction model

$$A(x) = \sum_{n=-\infty}^{+\infty} R^n Airy\left[(-1)^n \left(x - x_n\right)\right]$$

$$I_{diffraction}\left(x', x_0\right) = \left|\int_{-\infty}^{+\infty} A(x)\exp\left(i\frac{2\pi}{\lambda_0}\sqrt{\left(x'-x\right)^2 + L^2}\right)dx\right|^2$$

(6)

Airy(x) is the complex amplitude in the telescope diffraction PSF at the SH input that corresponds to the elementary source, after integration in the along slit direction and clipping by the slit edges. For a rectangular pupil the diffraction PSF is a product of a function of x with a function of y, so the integration removes the function of y and we have:

$$Airy(x) = \Pi\left(\frac{x}{w}\right)sinc\left(\frac{x}{\lambda F_{\#}}\right)$$

(7)

$$sinc(x) = \begin{cases} 1 & \text{if } x=0 \\ \dfrac{\sin(\pi x)}{\pi x} & \text{otherwise} \end{cases} \qquad \Pi(x) = \begin{cases} 1 \text{ if } x<1/2 \\ 1/2 \text{ if } x=1/2 \\ 0 \text{ if } x>1/2 \end{cases}$$

A(x) is the source complex amplitude distribution that is built from all the mirror images of this elementary source.

The sum and integral are both ranging from -∞ to +∞. However in practice, the required summation and integration domains are finite and must be a bit larger (e.g. +50%) than the summation domain that was used for the interference model, because light is diffracted outside of the geometrical beam cone. The Airy patterns far away from this interval can be included in the computation but they have a totally negligible contribution to the final intensity. To ensure an accurate computation, it is necessary to check with a few numerical tests that the integration domain has been sufficiently extended so that contributions from outside this interval stay very small and negligible.

Diffraction is computed with a Huygens integral, which gives a simple formula and has a significantly wider validity range than other treatments based on a paraxial approximation (such as in [4]). As we can see, the interference (equation (5)) and diffraction (equation (6)) models are consistent: it is possible to recover the interference model equation from the diffraction formula by replacing the Airy pattern with a Dirac function.

Finally, the pupil information is contained in the expression of the Airy pattern so the diffraction model is valid for all pupil shapes.

Both models can be easily adapted to include the variation of R with angle of incidence. For simplicity, the provided expressions in equations (5) and (6) do not include normalization factors that ensure conservation of energy. These factors are not needed to compute the ISRF. The losses induced by a finite reflection can be easily computed by performing two calculations, one with perfect reflectance ($|R|^2=1$) and one with the real reflection coefficient R. As we will see later, the interference model is less accurate and does not exactly conserve energy, so it is better to evaluate the SH losses with the diffraction model.

We provide on figure 5 a plot of the intensity measured at the SH exit with the two models. This plot was validated against other existing SH models, as well as with Zemax. We hope that it will be used as a benchmark and help readers to write and validate their own model. The vertical scale of the two curves is arbitrary and the curves have been adjusted so that their integrals are equal. The following parameters have been used:

-       Slit width w=120 μm, slit length L=4.8 mm, reflection R= -1 (dephasing equal to π)

-       F-number = 10, wavelength = 500 nm

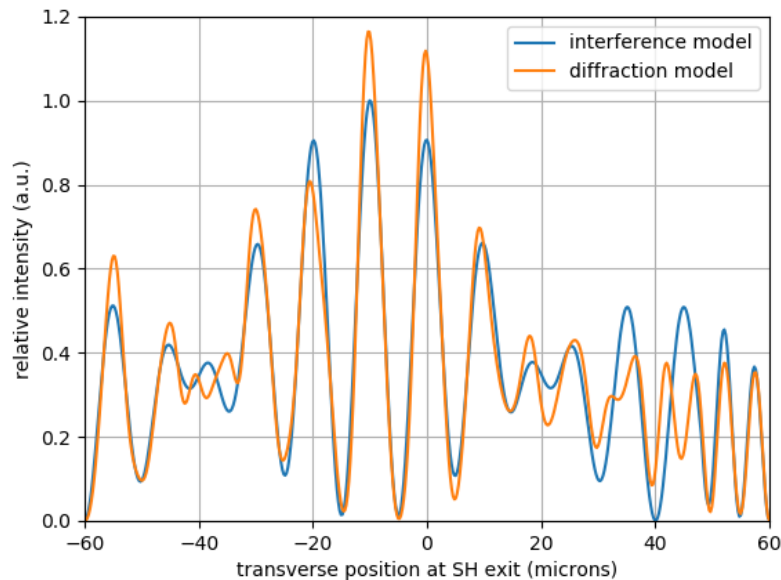-   Elementary source placed at x_0 = +48 μm

Figure 5. Example of intensity profile obtained at SH exit with the interference and diffraction models. See the text for the simulation parameters.
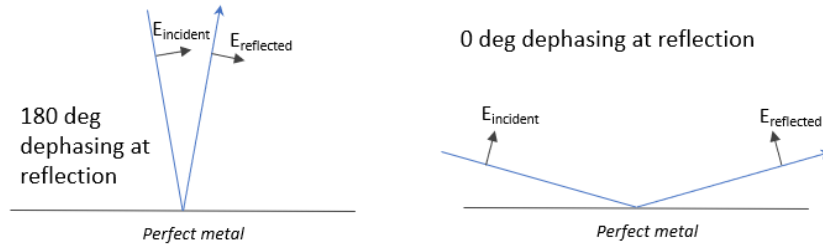
Figure 6. Using different conventions for the polarization axes in near-normal incidence geometry (left) and near-grazing incidence geometry (right) results in different dephasing definitions. For a perfect metal (infinite conductivity) the dephasing is 180deg at all angles (near-normal geometry convention), but it becomes 0deg with the convention for near-grazing geometry.

Care must be taken for defining the phase in the complex amplitude reflection coefficient R. While for s-polarized reflection (perpendicular to the plane of incidence) the phase definition is unambiguous, for p-polarized reflection (electric field inside the plane of incidence) there is a source of complication. To illustrate it, we take the example of a perfect metal (very large imaginary index). This material is convenient as the phase of R must be equal 180deg for all angles of incidence: it is required that the incident and reflected electric fields stay out of phase, so that the tangential (parallel to the interface) component of the electric field becomes zero at the interface and there is no electric field inside the metal. However, for a slit homogenizer with mirrors made of a perfect metal, while the phase shift is indeed 180 deg for s-polarization, a value of 0deg must be used in p-polarization. The reason for this change comes from the fact that the definition of phase shift must be modified for a geometry with grazing angles, as illustrated on the figure 6. The curves shown on figure 5 correspond to s-polarization over a perfect metal (180deg phase shift).
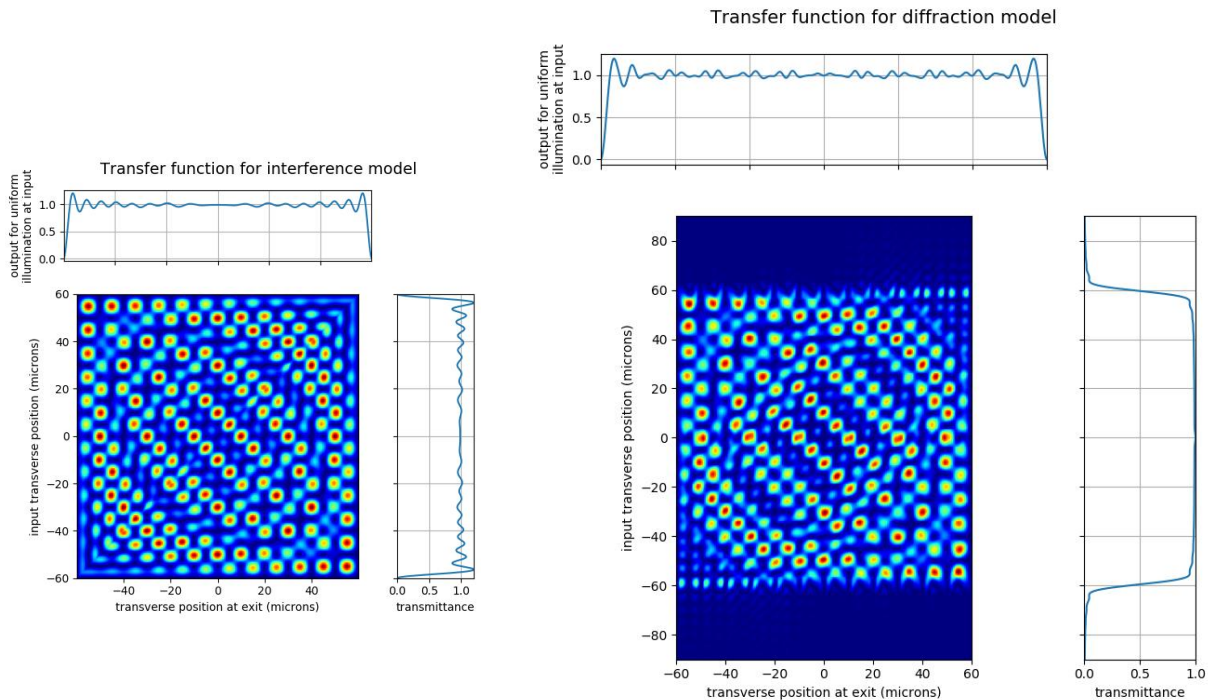

Figure 7. SH transfer functions obtained with the interference (left) and diffraction (right) models. See text for a detailed description. It is interesting to note that the transfer function computed with the diffraction model has less symmetries.

Given the equations of the two models, by varying x_0 and x' it is possible to compute the intensity distribution in the complete SH exit plane (all values of x') for any position of the elementary source at SH input (all values of x_0). If the slit width w is sampled with regular values of x_0 and x' it is possible to build a "transfer matrix" $M(x',x_0)$ that completely describes the behavior of the slit homogenizer. Then for a given distribution of elementary sources $S(x_0)$, the distribution of light at the SH exit $S(x')$ can be computed with:

$$S(x') = \sum_{\text{all } x_0} M(x', x_0) S(x_0).$$

(8)

The transfer matrices of the same SH as used for figure 5 (w=120µm, L=4.8mm, R=-1, F#=10, λ=500nm) have been computed with both interference and diffraction models, see figure 7. The two color maps for the interference and diffraction models are quite similar.

For the interference model the coordinates x_0 and x' must only span the width of the SH input and exit, both equal to w. In the case of the diffraction model, since the elementary source has a certain spatial extension (Airy pattern) it is necessary to compute the SH response for values of x_0 slightly outside the slit opening. If the Airy pattern center is outside of the SH opening, its diffraction wings can still enter the SH and be homogenized. This explains why the transfer function map is larger for the diffraction model.

In addition to the transfer matrix color maps, two plots are provided for each case:

- On the top of the main plots, the sum of $M(x', x_0)$ over x_0 is represented. It corresponds to the intensity measured at a certain coordinate x' in the SH exit plane, for a homogeneous illumination. The obtained curves can be used to compute the nominal ISRF, for the case when the observed scene is homogeneous.

- To the right of the main plots, the sum of $M(x', x_0)$ over all x' is shown. It provides the total transmitted intensity as a function of the position x_0 of the elementary source at input. This curve is therefore called "transmittance".

A few remarks shall be made about this "transmittance" plot. For the interference model, as we have simulated a SH with perfectly reflecting mirrors, and since the entire cone of light enters the SH and carries the same energy for each position of the elementary source at SH input, we would have expected a boxcar function for the transmittance curve. The transmittance should just be equal to 1 when the point source is inside the slit opening at SH input, and 0 if it is outside of the slit opening. Instead of that, we find a smooth and oscillating transmittance curve. It means that the interference model is slightly incorrect and does not exactly fulfill energy conservation. This error is a known limitation of interference models and has been observed in other contexts [7]. It is possible to correct it by scaling each intensity profile by a different factor in order to achieve the expected boxcar transmittance curve ; but the obtained intensity profile will still not be exact, and the amplitude of the correction factor gives an indication on the magnitude of the approximation that is done.

The best approach to solve these problems is to use the diffraction model (equation (6)). The diffraction model is more accurate and fulfills correctly conservation of energy. If it is used with perfectly reflecting mirrors and if the position of the elementary source (Airy pattern) at SH input is moved, as on figure 7, we find that the "transmittance" plot is still not a boxcar. The total amount of energy at SH exit then follows a smoothly varying curve, that gives exactly the fraction of the Airy pattern that enters the SH. As expected, the Airy pattern wings are clipped by the SH input edges and are not found in the intensity at SH exit.

The homogenizing performance of a SH device will depend on several factors:

- The blurring of the spatial information in the observed scene, due to satellite motion during integration time, and due to the telescope optical quality will reduce the impact of non-uniform scenes. It has been shown [5] that the ISRF distortion is proportional to the ratio between the slit footprint and the smear distance, both measured on ground. The worst case situation corresponds to a slit opening larger than the smear distance (ratio > 1). A ratio value around 0.5 is commonly used for pushbroom spectrometers. An instrument may be designed with a narrower slit opening (and therefore smaller ratio) to reduce the effects.

- The efficiency of the SH depends on the relative size of the diffraction pattern and the slit opening. The diffraction pattern has a size proportional to $\lambda.F_\#$, that corresponds to the size of one intensity peak in the transfer function (see figure 7). When the number of these peaks is increased in the transfer function, a better averaging takes place in the SH device.

- The role of the SH length is more complex. In principle, a minimum length must be used to achieve proper homogenization. Once the beam is reflected a few times on the SH mirrors, increasing further the length will not result in a significant improvement. The intensity pattern at exit contains several peaks (it is comparable to a random interference pattern like speckle) and will not get more homogeneous. When modelling the ISRF distortion as a function of SH length, an optimum performance has been predicted at regular lengths which reminds the "length rule" given by equation (3) (see e.g. [4]). Further analysis is required to confirm that these minima do not depend on the particular assumption used for input illumination.

2.3 Consequences of non-uniform pupil illumination

With the multiple reflections, the mirror-based SH will not only homogenize the slit but it will also modify the illumination of the system exit pupil. This can be seen easily by studying one elementary source point placed exactly at the upper edge of the SH opening (see figure 8).

This point emits light within a range of angles : any ray that goes upwards at a small angle will be immediately reflected downwards and pass through the slit homogenizer with only one reflection. It means that the part of the pupil that corresponds to small positive pupil coordinates is mirrored (x_{pup} is replaced by $-x_{pup}$). If the ray goes upward with a slightly larger angle, then it will be reflected 2 times before exiting the SH. With the 2 reflections it will recover its initial orientation and will exit the SH with its nominal direction. If we extend this reasoning, we can conclude that any ray that has underwent an odd number of reflections will have its pupil coordinate inverted. Based on this geometrical optics argument, we see that the pupil illumination will be significantly modified and will consist of "stripes".
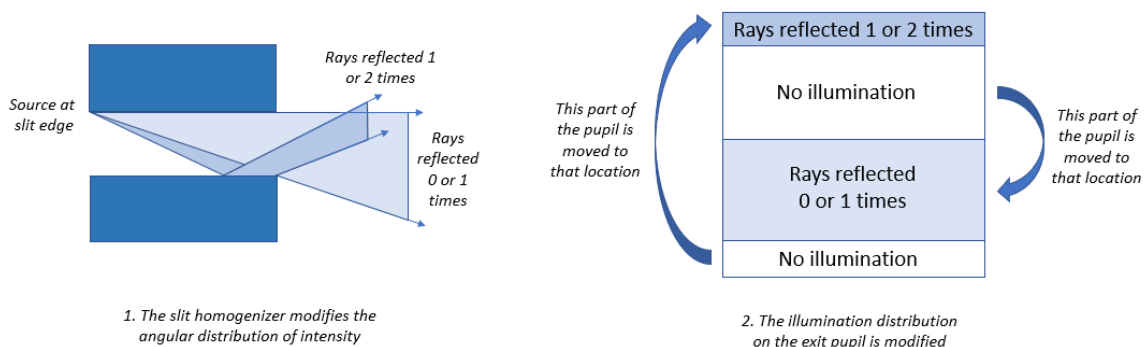

Figure 8. The multiple reflections in the mirror-based SH modify the angular distribution of intensity (left). As a result, the illumination on exit pupil is modified (right). This illustration is based on geometrical optics and is simplified, the reality is more complex and must account for diffraction and the interferences that occur when several beams are overlapping in the pupil plane.

The first question that comes to mind is the possible impact of this pupil illumination on the diffraction inside the spectrometer. The diffraction properties of a pushbroom instrument are not trivial, and have been analyzed in detail for the case of a regular slit in [8]. In that paper it is shown that the diffraction pattern obtained on the final image plane (where the detector is) depends on three things: the telescope pupil, the physical slit and the spectrometer pupil. The telescope pupil creates a standard diffraction pattern in the slit plane. The physical slit clips the wings of this diffraction pattern. Due to the clipping, a small amount of light is diffracted outside of the nominal range of angles that corresponds to the system F-number. To catch the diffracted rays, the spectrometer pupil must be slightly oversized, and the diffraction wings of the final optical spot obtained in the detector plane will depend on how much was the spectrometer pupil oversized. If the spectrometer pupil is large enough, all diffracted rays are re-imaged and the final image on the detector plane is an exact replica of the clipped diffraction pattern observed just after the slit, with a certain

magnification. In the limit of far-field diffraction the proof becomes simple and intuitive: two consecutive Fourier transforms are equivalent to an identity transformation with a minus sign. So if the spectrometer magnification is equal to unity then the final image on detector is identical to the illumination after the slit with a magnification equal to -1. In this idealized situation, there is no light on the detector outside of the image of the slit opening. The paper [8] indeed proved that thanks to the slit, the amount of diffracted light in a spectrometer is usually several orders of magnitude lower than the wings of a standard diffraction pattern.

When a mirror-based SH is used, it can be shown with a similar reasoning (based on diffraction integrals in the paraxial limit, and ignoring aberrations) that the modified illumination at the spectrometer pupil will not have any impact on the final image of the SH exit formed on the detector, as long as the grating, or any optical component in the vicinity of the spectrometer pupil, is slightly enlarged so that it does not "clip" the rays diffracted outside of the geometrical beams. In that respect, the diffraction behavior of the mirror-based SH is essentially similar to the behavior of a standard slit.

On the other hand, having a modified pupil illumination will have other consequences:

1.   the spectrometer aberrations will be different than in the nominal situation with a uniform pupil

2.   the spectrometer transmittance will be also modified

If we consider a given position of the elementary source point at SH input, the pupil illumination will be modified in a predictable way. In that case, these two errors are constant. Thanks to this property, they could be included in the transfer matrix that already contains the information about the interference pattern, and be used to compute a more accurate ISRF in presence of non-uniform slit illumination. Such generalized transfer matrix would not only describe the SH but also the spectrometer properties. Then equation (1) is no longer valid and the spectrometer PSF should be removed from it: the illumination computed from the transfer matrix should only be scaled to the right detector coordinates (using spectrometer magnification) and convolved with the detector PSF.

To our knowledge, very few attempts have been made to evaluate these two effects. They are usually ignored, due to the fact that with most instruments they only create small errors that are negligible as compared to the fluctuations of the interference pattern. Due to this, they can be considered as 2nd order errors. Ignoring them creates a small knowledge error in the properties of the SH and on the ISRF distortions, that will vary with the observed scene non-uniformity.

2.4 Combination with a polarization scrambler

We now discuss the consequences of combining a polarization scrambler [9] with the mirror-based slit homogenizer (this section is not essential to the general understanding of the paper and may be skipped in a first reading). As we will see, the polarization scrambler makes the SH modelling significantly more complex. A complete model description is not possible in the scope of this paper, therefore we will only provide a qualitative discussion of the most important aspects.

The SH performance model described in section 2.2 assumes that the telescope delivers either a perfect point-like optical spot (for the interference model) or a diffraction limited optical spot (for the diffraction model). It is possible to insert a more detailed description of the optical PSF in the diffraction model, for instance the optical spot diffracted by a more complicated aperture shape, or including some specific aberrations. To do it, it is only required to know the electric field amplitude distribution $A(x)$ in the slit plane and insert it in equation (6).

The situation gets more complex when the telescope includes a polarization scrambler. Typical scramblers (e.g. Dual Babinet) generate a 4 spot pattern in the slit plane. Let's call these spots A, B, C and D. They have linear polarizations in specific directions, and specific intensities that depend on the polarization state incident on the instrument. Each of these spots will undergo multiple reflections inside the SH, and will generate its own interference pattern at the SH exit. The complication comes from the fact that the interference patterns resulting from different spots may interfere with each other (e.g. the interference pattern created by A will interfere with the interference pattern created by C). To predict the performance of a slit homogenizer combined with a polarization scrambler, a more elaborate model is therefore needed that takes into account the 4 spots and their possible interactions.

Such a model should consider that two spots will only interfere with each other if the following conditions are simultaneously fulfilled:

(i)   the two spots are mutually coherent

(ii)　　　they don't have orthogonal polarization

(iii)　　they enter the slit homogenizer simultaneously

(iv)　　they have the same, or very close along-slit coordinates so that their final images overlap in the along-slit direction.

The condition (i) depends on the nature of the incident light. If the system is illuminated with a linearly polarized beam, then the 4 spots A, B, C and D are mutually coherent. If the incident light is unpolarized, then since the two orthogonal polarization components of unpolarized light are mutually incoherent, the final 4 spots pattern will be composed of two mutually incoherent pairs (A and B being coherent, C and D being coherent but the pair (A,B) being incoherent with (C,D), with A and B having orthogonal polarization, and C and D also having orthogonal polarization).

The criterium (ii) is intuitive but may be complex to evaluate in some situations. If the 4 spots have either horizontal (S) or vertical (P) polarizations, then after multiple reflections on the SH mirrors they will stay polarized in the same direction (S or P). This case is simple as S-polarized (resp. P-polarized) spots can only interfere with spots having the same polarization direction. On the other hand, the situation with 4 spots polarized at +/-45 deg at the SH input is more complicated. If the mirror reflectance is slightly different in S and P polarizations the 4 spots will have a slightly modified polarization direction at SH exit and new interference contributions may appear.

To evaluate condition (iii) it is necessary to compare the width w of the slit homogenizer to the separation between the two spots. If the spot separation is larger than w, the two spots cannot interfere because they cannot enter the slit homogenizer at the same time. For a system with a spot separation smaller than w, three situations will happen and must be considered when computing the performance: the two cases where only one of the spots enters the slit homogenizer (no interferences), and the case where the two spots enter simultaneously the SH and will produce interferences.

Finally, the condition (iv) is necessary to make sure that the two spots will not be imaged at different along-slit coordinates and that their overlap is sufficient to create interferences.

3. LENS-BASED SLIT HOMOGENIZER

3.1 Working principle

The lens-based SH relies on a very different principle. It makes use of the fact that, while the image in the telescope focal plane is not homogeneous, the telescope pupil is homogeneously illuminated. The lens-based SH will replace the slit image by an image of the telescope pupil in the across-slit direction.

To do that, it uses a cylindrical lens element (see figure 9). The cylindrical lens has no power in the along-slit direction, and has power in the across-slit direction. It can be a rod lens (in that case the lens section in across-slit direction is a disk), or can have any other shape (the section in across-slit can be the one of a plano-convex lens, a bi-convex lens, etc). In our discussion we will assume a rod lens, as the circular cross-section offers several advantages: the rod lens is a commercially available component (including AR coating) and has one rotational degree of freedom less to be controlled for mounting.
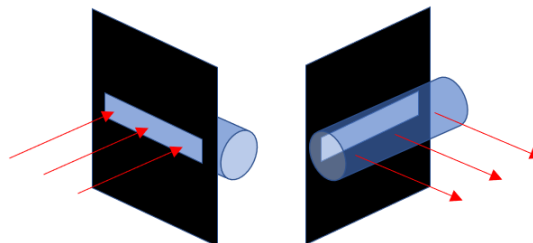
Figure 9. Typical implementation of the lens-based SH with a rod lens placed behind the physical slit.

In figure 10, the SH working principle is illustrated for the situation with telecentric illumination. In that case, an image of the telescope pupil is formed in the focal plane after the lens rod. This pupil image is homogeneous and plays the role of spectrometer entrance slit. We see that the exchange between image plane and pupil plane done by the SH is performed through a re-distribution of the rays. The red cone of light that comes out of the slit upper point, will contribute equally to the lower marginal rays of all field points after the SH.
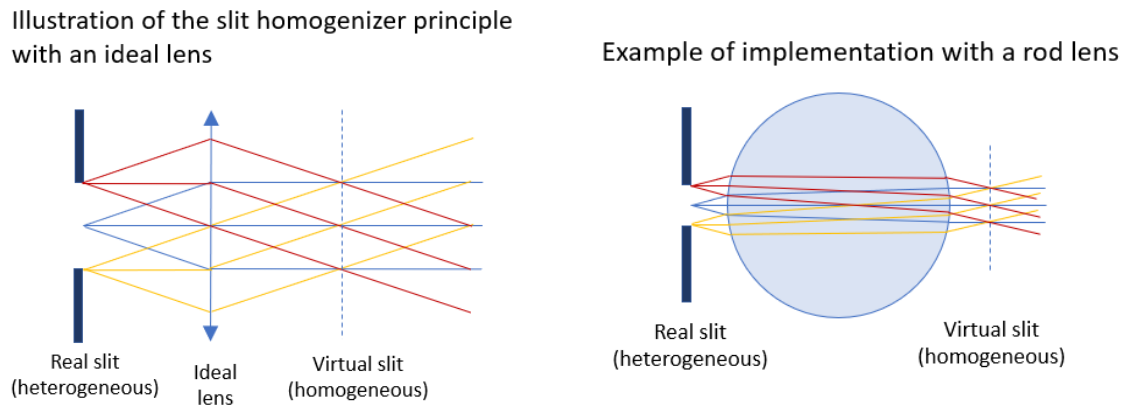

Figure 10. Left: principle of the lens-based SH, in a telecentric-telecentric situation (telescope beam is telecentric, and SH delivers a telecentric beam). The homogeneous virtual slit is an image of the telescope pupil. Right: practical implementation with a lens rod.

The SH can be also used with a telescope that delivers a non-telecentric beam, without design change and without any difference in its operating principle. The telecentricity (or non-telecentricity) of the beam after the SH is totally independent from the telecentricity (or non-telecentricity) of the beam coming out of the telescope. The telescope telecentricity defines the distance where the homogeneous slit image is formed after the SH. The telecentricity of the beam after the SH is controlled by the distance between the slit and the lens rod. We also note that the SH can be used indifferently with all pupil shapes without any design change.

In the same way as for the mirror-based SH, the lens-based SH requires an astigmatic optical system. In the across-slit direction the telescope is focused at the real slit, and the telescope pupil image, as relayed by the rod lens, is in the object plane of the collimator. In along-slit, the telescope and collimator must share a common focal plane, taking into account the fact that the lens rod will shift this focal plane for one of the two optical modules (telescope or collimator) due to the glass thickness.

3.2 Performance

In this paragraph, we will review all aspects that may limit the performance of the lens-based SH. As we can already see, if imaging through the lens rod and through the spectrometer are perfect, then a perfectly homogeneous slit image is formed after the SH and is imaged onto the final instrument focal plane. In that case, ISRF distortion is equal to zero and the problem of slit non-uniformity disappears totally.

A first effect that must be discussed is the longitudinal chromatic aberration of the lens rod. If the lens rod is composed of a single element, it cannot be chromatically corrected and has a variable focal length through the instrument spectral range. A first consequence is that the physical slit will be imaged differently through the lens rod for short and long wavelengths. As can be understood from figure 10, it means that the chief rays after the SH (in blue in the figure) will have different angles : they may be parallel as on the figure, or slightly diverge or converge for different wavelengths. In other terms, the pupil position after the SH will be slightly shifted longitudinally depending on wavelength. A second consequence is that the homogeneous slit image after the lens rod will be formed at different longitudinal positions. In a spectrometer, these effects (chromatic aberrations of both the image and pupil) can be easily corrected thanks to the wavelength separation after the grating, with the imager aberration correction and with a detector tilt. In the same way, geometrical aberrations will also degrade the slit image that is formed after the SH. As for chromatic aberrations, the

homogeneous slit image doesn't need to be perfect ; it can be corrected later in the spectrometer. In some way, the lens rod performs most of the work by shifting the image and pupil planes; the spectrometer will finalize the work by optimizing the optical quality of the final slit image on the detector. The overall quality of the slit image is determined by the complete system composed of the spectrometer and the SH.

What are the consequences of having a non-perfect slit image on the detector? Since the lens rod performs an exchange between image and pupil plane, after the SH the spectrometer pupil will become highly non-uniform. It means that rays will propagate differently through the spectrometer depending on the particular observed scene. If the spectrometer optical quality is perfect, this has no consequences: all the rays will end up at the same position on the final image plane independently of their pupil coordinate. If the spectrometer optical quality is not perfect, then these rays will have different aberrations depending on the pupil illumination, which means that the final slit image, and the ISRF will be distorted depending on the observed scene.

Such effect of variable spectrometer pupil illumination, resulting in variable aberrations in the final image, has been already discussed for the mirror-based SH. In the same way as for the mirror-based SH, it will also induce a radiometric error due to transmittance variations across the spectrometer pupil. It is important to note that this effect of variable transmittance will also occur if image quality is perfect. So to achieve an optimal SH performance it is not only necessary to design a spectrometer with a good optical quality, but also with a uniform transmittance over the pupil.

Note that geometrical distortions (similar to smile and keystone) or a non-uniform illumination of the final slit image (resulting from e.g. a variable transmittance across the telescope pupil, before the SH) will also affect the ISRF shape but since these are constant effects, they can be calibrated and will not create any scene-dependent ISRF distortion.

To conclude the discussion, the lens-based SH does not suffer from any 1st order limitation. Based on this, we expect that it has a significantly higher performance than the mirror-based SH. Its performance will be limited by the following 2nd order effects:

1. the variations of optical aberrations in the spectrometer with a non-uniform pupil illumination,

2. the radiometric error created by the non-uniform transmittance over the spectrometer pupil, with a non-uniform pupil illumination.

The performance of the lens-based slit homogenizer is therefore not an intrinsic quantity and directly depends on the properties of the spectrometer with which it is used. As already mentioned, very few attempts have been made to our knowledge to model such 2nd order effects for the mirror-based SH. To evaluate quantitatively the performance of the new type of SH will require the development of new models.

3.3 Comparison with mirror-based SH

To summarize the discussion, we provide an exhaustive list of pros/cons of each type of slit homogenizer. A small sign (++ or -) is inserted to evaluate the facility/benefits or difficulty/drawbacks of each approach. The lens-based SH seems very promising. Despite a more complex design of the spectrometer, we believe that it potentially offers a better performance and easier manufacturing.

SH type	Mirror-based	Lens-based
Difficulty of design	++ A small amount of astigmatism must be introduced in the system.	- A small amount of astigmatism must be introduced in the system. The chromatic and geometric aberrations of the lens rod must be corrected in the spectrometer.
Optical requirements	- Telecentric illumination at slit is desirable. Mirror-based SH has a better performance with a rectangular pupil.	++ The lens-based SH is more flexible. No requirement on telecentricity, can accommodate any pupil shape.

| Performance | -

Limited by the fluctuations of the interference pattern created by the multiple reflections. These fluctuations cannot be reduced below a certain limit.

The 2nd order effects, resulting from the non-uniform spectrometer pupil are smaller and usually disregarded. | ++

Intrinsically good performance.

Limited by the 2nd order effects, resulting from the non-uniform spectrometer illumination. |
|---|---|---|
| Modelling | ++

Based on transfer functions formalism. | -

Modelling has not yet been explored. |
| Manufacturing | -

A special coating with high reflectivity at grazing incidences must be developed.

The two mirrors are glass or metallic blocks assembled with spacers, making the SH a custom component. | ++

Lens rods with appropriate coatings are commercially available. |

4. CONCLUSION

The interest towards slit homogenizers in Earth observing imaging spectrometers is growing, due to more demanding requirements in terms of spatial resolution and radiometric accuracy in the new generation of instruments [4, 5, 10]. In this paper we summarize all the basic information necessary to design a mirror-based SH as used in Sentinel-5 and model its performance. We also present for the first time a new type of slit homogenizer based on a lens rod, that seems more promising in terms of performance and manufacturability.

A patent application was filed for this new SH design [11]. Its greater flexibility as compared to the mirror-based SH (no requirement on telecentricity or pupil shape), the fact that it may be built with off-the-shelf components makes it potentially attractive for use in commercial spectrometers for a broad range of applications, not only remote sensing. The only requirement is to form a good image of the exit pupil of the imaging or illumination system (called telescope in this paper) in the across slit direction on the final image plane. For some spectrometer designs where the illumination system is unspecified, it may be necessary to place a physical stop inside the spectrometer. When using a lens-based SH, two separate physical stops become then necessary: one stop (in the along-slit direction) should still be located around the spectrometer grating as in traditional designs; while the other physical stop (in the across-slit direction) should be placed just after the lens rod where the pupil exit image is expected. This second physical stop would act only in across-slit direction so it would be a second slit : the lens rod would have two slits (one on each side).

Besides the slit homogenizers discussed in the present paper, 2-dimensional slit homogenizers have been proposed for spectrometers used in remote sensing [12]. They are made of bundles of optical fibers with a square or rectangular cross-section, and homogenize the observed scene in both the across-slit and along-slit directions. These devices offer specific advantages in terms of performance: in particular they can correct the radiometric errors resulting from the combined effect of spectrometer smile and scenes spatial non-uniformities in the along-slit direction [5, 12]. They are based on the same principle as the mirror-based SH (homogenizing a beam with multiple reflections), with the optical fibers being the 2-dimensional counterpart of the SH mirrors. An alternative type of 2D slit homogenizers, using a similar approach as the new lens-based SH could be investigated. Such systems could rely on the use of an array of micro-lenses that create multiple images of the instrument pupil, to be used as virtual slits by the spectrometer placed behind it.

REFERENCES

[1] R.Voors, M.Dobber, R.Dirksen, P.Levelt, "Method of calibration to correct for cloud-induced wavelength shifts in the Aura satellite's Ozone Monitoring Instrument", Appl. Opt. 45, 3652-3658 (2006).

[2] S.Noël, K.Bramstedt, H.Bovensmann, K.Gerilowski, J.P.Burrows, C.Standfuss, E.Dufour, B.Veihelmann, "Quantification and mitigation of the impact of scene inhomogeneity on Sentinel-4 UVN UV-VIS retrievals", Atmospheric Measurement Techniques, vol.5, no.6, pp 1319-1331 (2012).

[3] This result was supported by results of scientific studies and was one of the starting assumption for the Sentinel-5 phase A-B1 study (ESA personal communication).

[4] Ch.Meister, C.Keim, J.Irizar, M.Bauer, "Sentinel-5/UVNS instrument: the principle ability of a slit homogenizer to reduce scene contrast for earth observation spectrometer", SPIE Proceedings Vol.10423, Sensors, Systems, and Next-Generation Satellites XXI; 104231E (2017).

[5] J.Caron, B.Sierk, J.-L.Bézy, A.Loescher, Y.Meijer, "The Carbonsat Candidate Mission: radiometric and spectral performances over spatially heterogeneous scenes", ICSO 2014 conference, Tenerife, Spain (2014).

[6] "Illumination system", European Patent Application EP1793278A2.

[7] W.N. Mathews, "Superposition and energy conservation for small amplitude mechanical waves", Am. J. of Phys., 54 (3), pp 233-238, 1986.

[8] R.Berlich, B.Harnisch, "Radiometric assessment method for diffraction effects in hyperspectral imagers applied to the Earth explorer 8 mission candidate FLEX", ICSO 2014 conference, Tenerife, Spain (2014).

[9] J.Caron, J.-L.Bézy, G.Bazalgette, B.Sierk, R.Meynart, M.Richert, D.Loiseaux, "Polarization scramblers in Earth observing spectrometers: lessons learned from Sentinel-4 and 5 phases A/B1", ICSO 2012, Ajaccio, France.

[10] B.Moore, "The GeoCarb Mission", 14th International Workshop on Greenhouse Gas Measurements from Space, Toronto, 8-10 May 2018. https://iwggms14.physics.utoronto.ca/documents/124/6.8_Berrien_Moore_mac.pdf

[11] European patent application No. 18186243.4, "Slit homogenizer device for spectrometers".

[12] B. Guldimann, K. Minoglou, "Smart slit assembly for highresolution spectrometers in space", Proc. SPIE 9754, Photonic Instrumentation Engineering III, 97540B (16 March 2016).